

Nuclear Targeting with an Auger Electron Emitter Potentiates the Action of a Widely Used Antineoplastic Drug

Sebastian Imstepf,[†] Vanessa Pierroz,^{†,‡} Paula Raposinho,[§] Matthias Bauwens,^{||} Michael Felber,[†] Thomas Fox,[†] Adam B. Shapiro,[⊥] Robert Freudenberg,[#] Célia Fernandes,[§] Sofia Gama,[§] Gilles Gasser,[†] Felix Motthagy,^{||} Isabel R. Santos,[§] and Roger Alberto^{*,†}

[†]Department of Chemistry and [‡]Institute of Molecular Cancer Research, University of Zurich, Winterthurerstrasse 190, CH-8057 Zurich, Switzerland

[§]Centro de Ciências e Tecnologias Nucleares, Instituto Superior Técnico, Universidade de Lisboa, Estrada Nacional 10 km 139.7, PT-2695-066 Bobadela LRS, Portugal

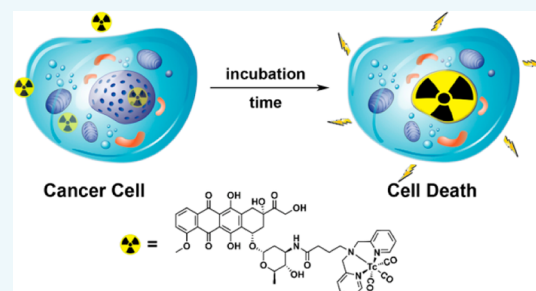
^{||}Department of Nuclear Medicine, MUMC+, P. Debeyelaan 25, NL-6229 Maastricht, Netherlands

[⊥]Bioscience Department, Infection Innovative Medicines, AstraZeneca R&D Boston, Waltham, Massachusetts 02451, United States

[#]Universitätsklinikum Carl Gustav Carus Dresden, Fetscherstrasse 74, D-01307 Dresden, Germany

Supporting Information

ABSTRACT: We present the combination of the clinically well-proven chemotherapeutic agent, Doxorubicin, and ^{99m}Tc, an Auger and internal conversion electron emitter, into a dual-action agent for therapy. Chemical conjugation of Doxorubicin to ^{99m}Tc afforded a construct which autonomously ferries a radioactive payload into the cell nucleus. At this site, damage is exerted by dose deposition from Auger radiation. The ^{99m}Tc-conjugate exhibited a dose-dependent inhibition of survival in a selected panel of cancer cells and an in vivo study in healthy mice evidenced a biodistribution which is comparable to that of the parent drug. The homologous Rhenium conjugate was found to effectively bind to DNA, inhibited human Topoisomerase II, and exhibited cytotoxicity in vitro. The collective in vitro and in vivo data demonstrate that the presented metallo-conjugates closely mimic native Doxorubicin.



INTRODUCTION

Auger and internal conversion electron therapy is a particular form of radionuclide therapy (RNT), which uses low energy electrons from radionuclides to destroy malignant cells. Importantly, the delivery of therapeutic radiation doses in Auger electron therapy occurs over molecular to subcellular dimensions. The path lengths of Auger electrons contrast those of α - and β -particles, which deposit their energy in the form of evenly distributed ionizations over submillimeter to millimeter ranges, thereby exposing multiple cells along their tracks to radiation—a phenomenon referred to as the “cross-fire effect”.¹ As tissue has a particularly high stopping power for the low energies carried by Auger electrons (eV to low keV range), their total energy is deposited along ultrashort particle tracks. This large linear energy transfer (LET) causes ionizations and electron showers which lead to massive radiation damage along path lengths of subcellular dimensions. Hence, Auger and internal conversion electrons exhibit a relative biological effectiveness (RBE) similar to that of heavy charged particles.² Vice versa, these ultrashort trajectories have implications regarding the application of these emitters as decay events must take place right at the target (or in its immediate vicinity)

to show any effect. Since nuclear DNA is the primary radiosensitive target, Auger emitters must accumulate in the cell nucleus and integrate in or attach to the double helix to inflict radiation damage in the form of irreparable double strand breaks (DSBs). In previous studies, conjugation of Auger emitters to nucleobases,^{3–6} (anti-)hormones,^{7,8} or intercalators⁹ effected this damage. Reviews by Hofer¹⁰ and Kassis¹¹ comprehensively describe the biophysical aspects of Auger emitters.

^{99m}Tc is a widely used radionuclide in nuclear medical SPECT imaging with a half-life time of 6 h.^{12,13} Besides the emission of a 140 keV γ -quant (yield = 89%), it concomitantly ejects an average of four Auger electrons and ~ 0.11 internal conversion electrons per decay. The Auger electrons of ^{99m}Tc with the highest theoretical probability of inducing DSBs in DNA are shown in Table 1.¹⁴

Earlier reports experimentally confirmed the potential of ^{99m}Tc for Auger electron therapy, in cell free systems,^{15,16} and

Received: August 25, 2015

Revised: October 9, 2015

Table 1. Average Energy, Yield/Decay and Tissue Penetration Range of the Most Probable Electrons Emitted by ^{99m}Tc for the Induction of DSBs

average energy [eV]	yield per decay	tissue penetration range [nm]
116	0.75	6
226	1.1	10.5
33	1.98	2

in vitro, employing intercalators such as pyrene¹⁷ or anthracene derivatives.¹⁸

Doxorubicin (ADR), a natural, broadband chemotherapeutic agent, is an anthracene derivative, known to intercalate strongly between DNA nucleobases.^{19–21} ADR is clinically well-proven and shows extensive activity against a variety of cancers.^{22–24} Its mode of action is ascribed to the inhibition of Topoisomerase II and to the resulting damage during DNA replication, inducing apoptosis, the programmed form of cell death.²⁵ Like many anticancer drugs, ADR causes serious off-target adverse effects; immunosuppression hampers the quality of life of patients and the dose dependent, acute cardiotoxicity greatly reduces therapeutic margins.^{26,27} To improve the efficacy of ADR, strategies to enhance delivery and reduce toxicity have been exploited, e.g., by delivery with (pegylated) liposomes^{28–30} or in hydrogels,^{31,32} derivatization of nanoparticles,^{33–37} and direct administration of modified ADR derivatives³⁸ or prodrugs.^{39–42}

Inspired by the clinical relevance of ADR, we present in this study the first well characterized Doxorubicin- ^{99m}Tc conjugate (**1**, Scheme 1) which was scrutinized for radiotoxic effects in multiple cancer cell lines. In situ, the characterized “cold” rhenium surrogate **2** was found to bind to DNA and to inhibit human Topoisomerase II α and β . Furthermore, the model Re complex retained cytotoxicity toward a human cancer cell line in vitro. Cellular localization and nuclear targeting were studied with confocal fluorescence microscopy, and the subcellular distribution of the ADR-conjugates was corroborated by two individual quantification methods: radioactivity and inductively coupled plasma mass spectrometry (ICP-MS). Moreover,

imaging with a small animal microSPECT and an ex vivo biodistribution study in nude NMRI mice were carried out to elucidate the behavior of radioactive complex **1** in vivo.

RESULTS AND DISCUSSION

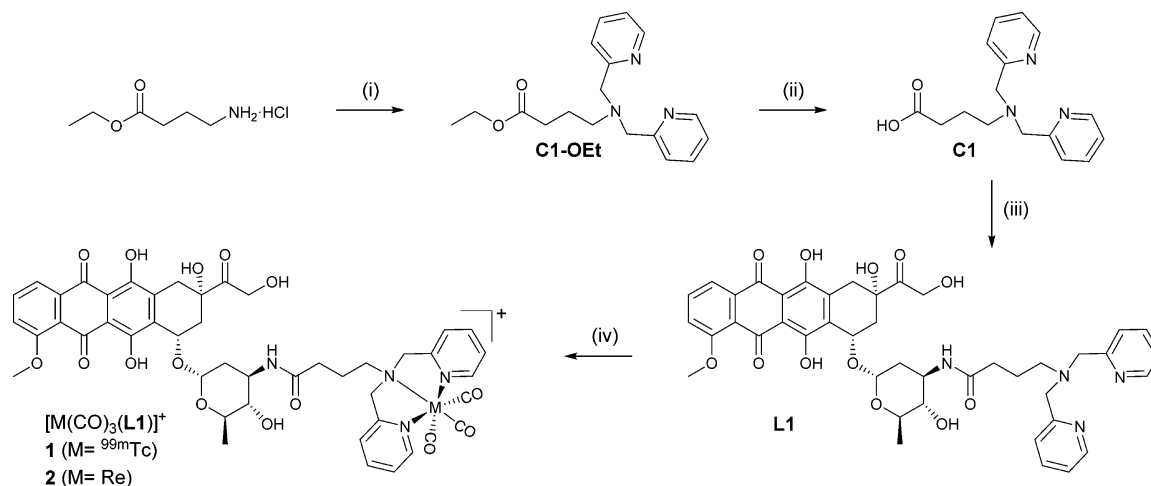
Design and Synthesis of the ADR-Conjugates.

Conjugates **1** and **2** (Scheme 1) were designed according to the bifunctional chelator (BFC) concept.⁴³ The biological vector (ADR) is conjugated via a linker to the dipicolylamine chelator, which binds strongly to the *fac*- $\{\text{M}(\text{CO})_3\}^+$ core ($\text{M} = \text{Re}/^{99m}\text{Tc}$). ADR, a strong intercalator, was chosen to spatially fix the radionuclide to DNA in order for the decay to induce DSBs via energy transfer by emitted Auger and internal conversion electrons. The positive charge on the complex should induce ionic interactions with the negatively charged phosphate backbone to bring the radionuclide close to DNA.

Chelator **C1** was synthesized by reductive amination of ethyl 4-aminobutyrate hydrochloride with an excess of picolinaldehyde and sodium triacetoxyborohydride (STAB) as reducing agent.⁴⁴ After basic hydrolysis of **C1-OEt**, bifunctional ligand **L1** was obtained in 44% overall yield (3 steps, SI Charts S1–S3), by a HBTU mediated amide bond formation with commercially available ADR-HCl. **L1** was fully characterized by detailed NMR studies (see Charts S4–S6) and high-resolution mass spectrometry (HR-ESI⁺).

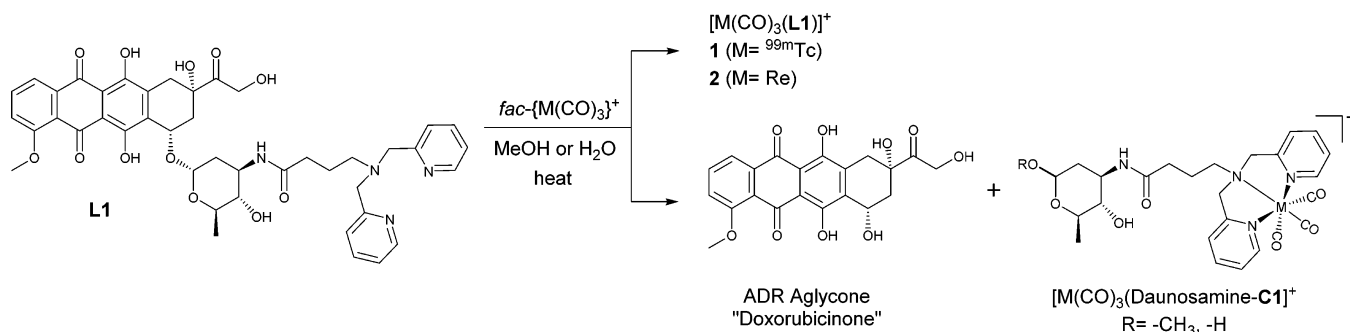
For characterization of ^{99m}Tc products at the tracer level, coinjection with the “cold” rhenium homologue is an accepted procedure for the unambiguous authentication of a new radioproduct. Consequently, rhenium complex **2** was prepared by reacting **L1** with the standard precursor $(\text{NEt}_4)_2[\text{ReBr}_3(\text{CO})_3]$ in MeOH. Temperatures above 60 °C and prolonged heating led to methanolysis of the α -glycosidic bond, resulting in the ADR-aglycone (Doxorubicinone) and metalated daunosamine sugar moiety (Scheme 2). Both degradation products and their respective masses were identified via UPLC-ESI⁺ (see Chart S7). After optimization of the conditions, **2** was obtained in 63% yield after purification and fully characterized by NMR studies (see Charts S8–S12).

Scheme 1. Synthesis of ADR Conjugates **1** ($\text{M} = ^{99m}\text{Tc}$) and **2** ($\text{M} = \text{Re}$)^a



^a(i) 2-Pyridinecarboxaldehyde, STAB, TEA, CH_2Cl_2 , 25 °C, 86%; (ii) 0.1 M NaOH, H_2O , 85 °C, 84%; (iii) ADR-HCl, HBTU, DIPEA, DMF, 25 °C, 61%; (iv) **1**: $[\text{M}(\text{CO})_3(\text{L1})]^+$, H_2O , 60 °C, 70% radiochemical yield (RCY), **2**: $(\text{NEt}_4)_2[\text{ReBr}_3(\text{CO})_3]$, MeOH, 60 °C, 63%. STAB = sodium triacetoxyborohydride, TEA = triethylamine, DIPEA = *N,N*-diisopropylethylamine, HBTU = *N,N,N',N'*-tetramethyl-*O*-(1*H*-benzotriazol-1-yl)uronium hexafluorophosphate, DMF = *N,N*-dimethylformamide.

Scheme 2. Solvolysis of L1 during the Synthesis of Conjugates 1 (M = ^{99m}Tc) and 2 (M = Re) to the ADR Aglycone (Doxorubicinone) and the Metalated Daunosamine Sugar by Coordination to $\text{fac-}[M(\text{CO})_3]^+$ (M = $^{99m}\text{Tc}/\text{Re}$) in MeOH or H_2O



The α -glycosidic bond is indeed the most sensitive part of ADR, and cleavage of the daunosamine sugar is part of the metabolic pathway of the parent drug.^{24,45,46} In vivo, this hydrolysis is proton-catalyzed, whereas under our reaction conditions, the Lewis-acidic $\text{fac-}\{\text{Re}(\text{CO})_3\}^+$ fragment is likely to cause methanolysis. We note that labeling experiments, under fully aqueous conditions, with ^{99m}Tc showed a similar behavior (vide infra). Metal derivatives of ADR are relatively scarce but have been reported for Fe(III),^{47–50} Mn(II),⁵¹ Cu(II),⁵² Pt(II),⁵³ Co(II),⁵⁴ and Pd(II).⁵⁵ Most of these complexes, however, are formed in situ and are poorly characterized. Complex 2 is, to the best of our knowledge, the first Doxorubicin–metal conjugate.

During labeling of L1 with the $\text{fac-}\{^{99m}\text{Tc}(\text{CO})_3\}^+$ core, a significantly more hydrophilic side product (yield ~ 10 – 15%) was observed at elevated temperatures. By analyzing the aqueous degradation products of surrogate 2 and coinjection, we attributed this impurity to the labeled daunosamine-chelator construct (see Scheme 2). Since most unlabeled L1 remained intact, the side product likely forms at the tracer level by α -glycosidic bond cleavage of 1. Side product formation was suppressed to some extent by acidic quenching of the kit-contained sodium boranocarbonate and subsequent readjusting of the $[\text{Re}(\text{CO})_3(\text{OH})_2]^+$ precursor solution to pH 6–7 before labeling of L1. The pH window to label ADR in aqueous media is narrow: Below pH 6, glycosidic cleavage is promoted and above pH 7, L1 precipitated from the aqueous solution.

Under optimized conditions, conjugate 1 was obtained in excellent turnovers from $[\text{Re}(\text{CO})_3(\text{OH})_2]^+$ and in a radiochemical purity (RCP) of around 85–90% (see Chart S13). For biological evaluations, the crude reaction mixtures were purified by HPLC to afford a RCP $\geq 95\%$. Co-injection and comparison of the HPLC retention time with homologue 2 confirmed the identity of ^{99m}Tc -complex 1 (Figure 1, difference due to detector separation). Of note, an attempt to directly radiolabel ADR (no pendent chelator) with ^{99m}Tc has been reported before by stannous(II) chloride reduction of $[\text{Re}(\text{CO})_4]^-$ in the presence of ADR. Yet, authenticity of the product has not been determined.⁵⁶

Biological Data. To establish an in situ and in vitro profile, the cold rhenium conjugate 2 was subjected to a variety of biological assays the results of which are summarized in Table 2.

Interaction with DNA. DNA is the primary target of Auger radiation. Hence, the radionuclide needs to sojourn closely around DNA over the time of its decay, as theoretical calculations indicated precipitous dose reductions for Auger

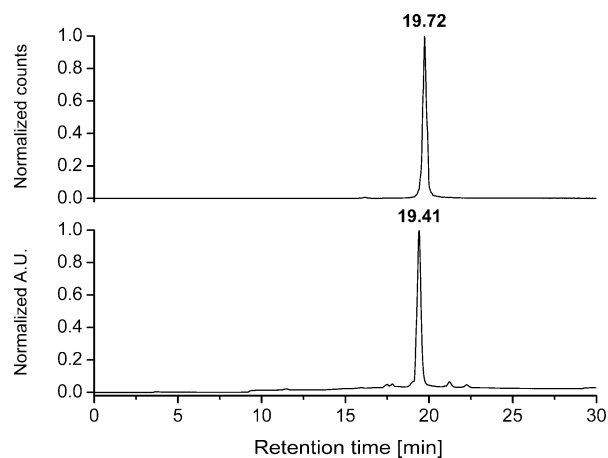


Figure 1. Normalized HPLC coinjection after purification. Top: γ -trace of 1 (19.72 min, RCP $> 98\%$ as determined by integration). Bottom: UV-trace of rhenium complex 2 (19.41 min).

emitters located at increasing distances from the DNA central axis.^{9,57,58} Since ADR and related anthracycline drugs are strong intercalators,²¹ incorporation of this targeting moiety in compound 1 should afford ^{99m}Tc decays in the intimate proximity of DNA, resulting in an efficient energy transfer. The binding affinity of 2 for double-stranded DNA is therefore a decisive parameter. Since ADR's fluorescence is quenched upon intercalation, the changes in the emission spectrum of complex 2 were monitored upon titration with calf-thymus DNA (ctDNA).⁵⁹ The spectroscopic data allowed F_{bound} (fraction of intercalator bound to DNA) to be calculated and was fitted to the equation by Bard et al. to obtain the binding constant (K_b) and the size of the interaction site (s).^{60,61} The K_b and s values for 2 are reported in Table 2 along with free ADR as a reference (see also Charts S14 and S15). The initial fluorescence of derivative 2 in PBS (pH 7.4) is maximal in the absence of ctDNA and is strongly quenched at increasing DNA concentrations. No shift in the emission maximum (593 nm) was observed. Evidently, the DNA binding constant of 2 is one order of magnitude smaller than that of free ADR. We attribute this decrease to the derivatization at the daunosamine- NH_2 , which is known to be critical for DNA interaction.⁶² Nevertheless, the value obtained indicates a strong interaction of 2 with DNA.

Inhibition of Cellular Proliferation (Chemotoxicity) and Topoisomerase II. The chemotoxicity of ADR-conjugate 2 was investigated by a fluorometric cell viability assay

Table 2. In Situ and In Vitro Biological Data of Rhenium Complex 2 and ADR

	DNA binding ^a		Human Topoisomerase II inhibition ^b IC ₅₀		Cytotoxicity after 48 h ^c IC ₅₀	
	K _b (M ⁻¹ per nucl) × 10 ⁶	s (bp)*	hTOPOII α (μM)	hTOPOII β (μM)	HeLa (μM)	B16F1 (μM)
Cisplatin	n/a	n/a	n/a	n/a	9.6 ± 1.1	20.6 ± 1.6
ADR	4.98 ± 0.45	2.00 ± 0.04	1.6 ± 0.2	1.1 ± 0.02	0.093 ± 0.02	0.095 ± 0.01
2	0.23 ± 0.03	2.20 ± 0.15	9.7 ± 1.2	4.5 ± 0.6	19.7 ± 2.1	11.4 ± 4.9**

^aK_b: affinity constant for DNA; s: binding site size; *bp: base pairs. ^bValues indicate means ± standard deviations of triplicate experiments made for the enzymes side by side. ^cValues indicate means ± standard deviations of triplicate experiments; cisplatin was used as internal reference; **duplicate experiment only.

(Resazurin). The IC₅₀ of complex 2 toward the standard human cervical cancer (HeLa) cell line was determined to be 19.7 μM after 48 h of incubation (Table 2). This inhibitory potency is significantly reduced compared to native ADR which exhibited an IC₅₀ in the high nanomolar range. It is a known phenomenon that amine group derivatization reduces cytotoxicity, which is currently under investigation for new drug delivery mechanisms via bio-orthogonal prodrug activation.^{41,63} On the other hand, the IC₅₀ of 2 was determined to be in the same range as cisplatin (internal reference), exemplifying that the metal-conjugate retains a potentially useful cytotoxicity in vitro. Of note, in recent years *fac*-{Re(CO)₃}⁺-complexes were shown to have interesting properties as anticancer agents.^{64–67} With optimizations, ADR could indeed be a lead structure for inorganic drugs or delivery thereof, possibly exploiting new cytotoxic mechanisms.

While different mechanisms of action are discussed in the literature, it is accepted that ADR is a strong inhibitor of human topoisomerase II (hTopoII).⁶⁸ It was hence of interest to investigate if 2 would follow the same mechanism, despite the chemical derivatization of the parent pharmacophore. Accordingly, the ability of 2 to inhibit hTopoII α and β was determined by the method of Shapiro et al.^{69,70} This assay exploits the preferred binding of a fluorescently labeled oligonucleotide (TTC)₃T to double-stranded plasmid DNA, containing the triplex forming sequence (TTC)₉, after relaxation by hTopoII α or β versus the supercoiled plasmid. Changes in fluorescence anisotropy were monitored in the presence of inhibitor 2 at increasing concentrations to calculate the %-inhibition. The IC₅₀ was determined by nonlinear least-squares fit of the data points to an adaptation of the Hill equation. SI Chart S16 shows the concentration-dependent inhibition of hTopoII α and β by complex 2. As indicated in Table 2, ADR-conjugate 2 inhibits hTopoII α and β in concentrations comparable to the parent drug, and the slight selectivity of inhibiting hTopoII β more effectively than the α isoform is equally conserved. The marginally reduced inhibitory potency of 2 in comparison to free ADR is consistent with the reduced cytotoxicity of 2 in HeLa cells compared to the parent drug (vide supra).

Cellular Localization and Distribution. Effective nuclear accumulation is crucial for an Auger emitter since only decays in the nucleus are radiotoxic.^{71–74} ADR's fluorescence properties (λ_{abs} = 488 nm, λ_{em} = 592 nm) allow for determination of cellular distribution and localization of 2 by confocal microscopy. Figure 2 displays the fluorescence distribution of 2 (60 μM) after 2 h of incubation in HeLa cells. Fluorescence was observed in the cytoplasm and in the perinuclear region. No nuclear accumulation of fluorescence could be detected while reference experiments with free ADR exhibited the red fluorescence exclusively in the nucleus (see Chart S17). Closer scrutiny of the images revealed a weak fluorescence signal in the

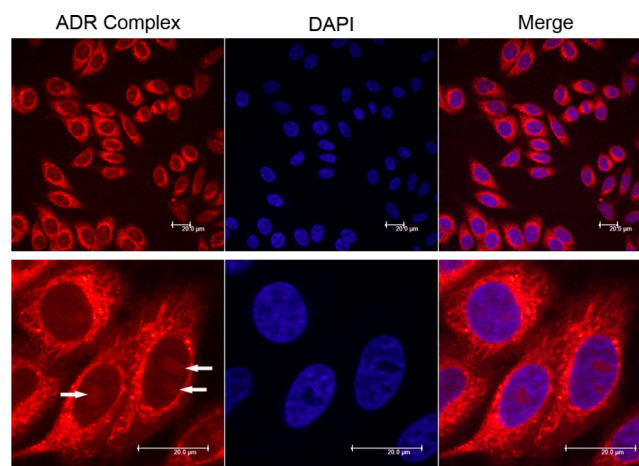


Figure 2. Confocal fluorescence microscopy of ADR conjugate 2 (60 μM) in HeLa cells after 2 h incubation. Left: ADR complex fluorescence (excitation at 488 nm, emission above 600 nm), center: DAPI nuclear stain, right: merge of complex 2 and DAPI staining. DAPI = 4',6-Diamidin-2-phenylindol. White arrows indicate fluorescence in nucleoli.

nucleoli (white arrows in Figure 2), indicating that conjugate 2 crossed the nuclear membrane. Since nucleoli contain RNA, we hypothesized that no intercalation takes place in these organelles and fluorescence is not quenched. Conversely, DNA intercalation may completely quench the fluorescence in the nucleus if 2 is fully intercalated. According to the literature and in our own experience (see Chart S14), ADR's fluorescent properties indeed depend on their microenvironment.⁷⁵ Thus, fluorescence microscopy might not always display the accurate cellular distribution of compounds, which dynamically alter their luminescence properties according to their surroundings. A clear picture can only be obtained by a complementary analytical technique such as determination of the radioactivity inside cellular compartments, which allows for a very sensitive quantification of metal traces.

A small panel of cancer cell lines, namely, human cervix carcinoma (HeLa), human squamous carcinoma (A431), and murine melanoma (B16F1), were incubated with radioconjugate 1. After removal of unbound compound by washing with PBS, nuclei and mitochondria were isolated from whole cells. The radioactivity in the nucleus and mitochondria pellets was then determined by a dose calibrator and expressed relative (%) to the activity in the whole cell pellet. In contrast to the results of fluorescence microscopy, these experiments showed that ^{99m}Tc complex 1 accumulates mainly in the nuclei (~75–80%) and to a minor extent in mitochondria (~1–2%). Moreover, no significant differences in the distribution of the conjugates were observed between the three cell lines. These distributions directly opposed the insights from confocal

microscopy and demanded confirmation by a third analytical method. Rhenium homologue **2** was therefore incubated separately, in the same cell lines and the Re content in the nuclei and mitochondria determined by ICP-MS, after digestion of the fractions by aqua regia. Figure 3 summarizes

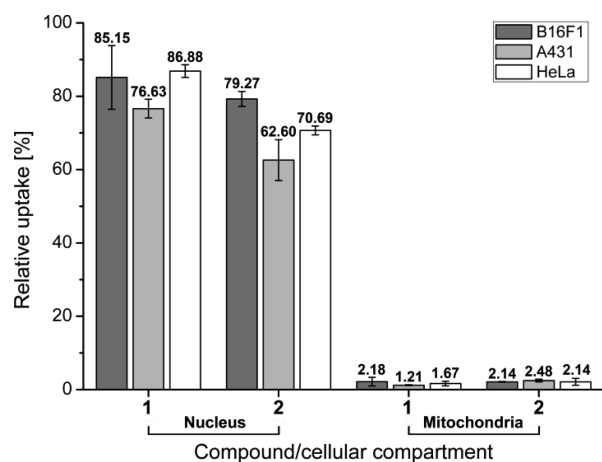


Figure 3. Relative uptake of **1** and **2** into nucleus and mitochondria compared to whole cell uptake for B16F1 (gray), A431 (light gray), and HeLa (white) cell lines. Quantification was done by a dose calibrator for **1** and ICP-MS for **2**. Values indicate means and error bars the standard deviations of six replicates for **1** and three replicates for **2**.

these results. The cellular distribution of **2**, according to ICP-MS, coincides very well with the distribution obtained for radioconjugate **1**: About 70–80% accumulates in the nucleus, whereas only a minor portion of rhenium is found in the mitochondrial fraction (~2%).

The quantitative data from ICP-MS and gamma-counting (absolute uptake values, see Chart S18) diametrically contrasted those of confocal microscopy, as fluorescence did not imply a major accumulation in the nuclei (vide supra). Both of the latter analyses clearly support the hypothesis that ADR conjugate **2** indeed accumulates mainly in the nuclei but cannot be visualized due to fluorescence quenching. According to ICP-MS, the concentration of **2** in the cell nucleus can be calculated to be about 33 μM —three orders of magnitude lower than the nuclear concentration of DNA base pairs. Since the fluorescence signal of ADR is quenched >95% at a roughly 50-fold molar excess of DNA base pairs, the fluorescence of **2** must be completely quenched under the conditions prevailing in the nucleus. Vice versa, the nuclear concentration of free ADR can reach up to 340 μM ,⁷⁶ sufficient to cause an excess fluorescence signal, as observed in the reference experiments with the parent ADR. Notably, the nuclear uptake of **2** is about 10-fold lower as compared to native ADR. Also, this observation is in agreement with the reduced potency of conjugate **2** to inhibit cell survival, as shown above. We do emphasize the remarkable agreement of relative uptake values of **1** (^{99m}Tc) and **2** (Re), determined by different quantification modalities. Whereas the chemical matched-pair behavior of ^{99m}Tc and Re is frequently quoted,^{77,78} our results demonstrate for the first time a biological matched-pair relation of rhenium and technetium. This largely equivalent in vitro behavior corroborates the homology of the two elements not only in chemistry, but also in biology.

Radiotoxicity and Mode of Cell Death. Cellular distribution and localization evidenced that **1** and **2** closely mimic the parent drug's in vitro behavior. The predominant nuclear accumulation of the conjugates and strong DNA binding indicated that Auger electrons from **1** could indeed effect radiologic damage. Accordingly, HeLa, A431, and B16F1 cell lines were incubated with different activity concentrations of **1** ranging 0–9.25 MBq/mL. For comparison with cold rhenium, the highest activity concentration corresponds to a solution which is about 1 nM in ^{99m}Tc+⁹⁹Tc, the latter resulting from the ^{99m}Tc transition to the ground state. As a negative control, [^{99m}TcO₄]⁻ was incubated at the maximum activity concentration, since the [^{99m}TcO₄]⁻ ion is not efficiently internalized into cells and should not exhibit a radiotoxic effect.^{17,79} After 36 h, the fraction of viable cells was determined by the MTT colorimetric assay to determine the cell line's radiosensitivity toward Auger electrons from **1**. As evident from Figure 4, complex **1** induced an activity-dependent inhibition of

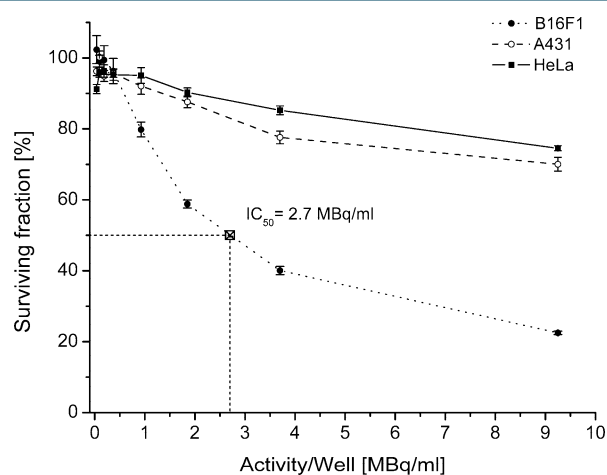


Figure 4. Surviving fraction (%) as a function of the activity concentration (0–9.25 MBq/mL) of radioactive ADR conjugate **1** in HeLa (■), A431 (○), and B16F1 (●) cell lines. Inhibitory potency (IC_{50}) of **1** in B16F1 cells is 2.7 MBq/mL. Symbols indicate means \pm standard deviations of eight replicates.

viability and a markedly radiotoxic effect in murine B16F1 cells which was less pronounced in the human cancer cell lines. At the maximum activity concentration of ca. 10 MBq/mL, we found 22.5% (B16F1), 70.0% (A431), and 74.5% (HeLa) of viable cells. At the same concentration, [^{99m}TcO₄]⁻ exhibited almost no radiotoxic effect: The survival was nearly 90% for all three cell lines (see Chart S19), reflecting the inability of this compound to reach the nucleus. This finding underlines the limited effectiveness of ultrashort path length radiation with increasing distance from the DNA target. However, the still non-negligible viability reduction might result in part from a dose deposition by conversion electrons. Although these account only for 11% probability, their range is between 200 and 400 μm , which is sufficient to reach the nucleus. We note that the radiotoxicity of **1** was less pronounced in the human cell lines, although overall uptake and cellular distribution were nearly identical. Variations in accumulation of radioactivity can therefore not be responsible for the observed differences in viability. Conversely, the response of cells from different tissues to radiation is known to be heterogeneous and depends on the intrinsic radiosensitivity, i.e., the ability of cells to detect DNA damage and the repair pathways associated therein.^{80,81}

From Figure 4, the IC_{50} of **1** in B16F1 cells was determined to be 2.7 MBq/mL, corresponding to a molar concentration of 1.41×10^{-10} M. In a previous study Haefliger et al. indicated an IC_{50} of 1.8×10^{-9} M in the same cell line for a pyrene derivative and proposed that this value could be significantly lower if a more effective nuclear targeting agent was found.¹⁵ In the present study, this value is now indeed 1 order of magnitude lower. Since the IC_{50} of ADR in B16F1 cells is in the submicromolar range (see Table 2), it is evident that radiotoxicity can be several orders of magnitude more effective in inhibiting cell survival than chemotoxicity. By determining the nuclear radioactivity in the subcellular compartments (vide supra), only 600 molecules of **1** accumulated in a cell's nucleus and are the cause of the observed radiotoxic effects in the B16F1 cell line. For comparison reasons, about 10^8 molecules of native ADR account for the above-mentioned nuclear concentration of 340 μ M. The unique combination of an Auger emitter with ADR, an effective nucleus targeting vehicle, therefore significantly potentiates the cell killing ability of the parent drug.

To investigate the cell death pathway induced by **1**, the B16F1 cell line was subjected to an Annexin V-FITC (An)/Propidium iodide (PI) assay. Cells were exposed to **1** at increasing activity concentrations of 1, 2, and 10 MBq/mL or 5 nM Staurosporin, a benchmark drug known to induce apoptosis.⁸² After an incubation period of 72 h, the percentage of apoptotic and necrotic cells was determined by fluorescence-activated cell sorting (FACS, representative histograms are shown in Chart S20). As evident from Figure 5, the percentage

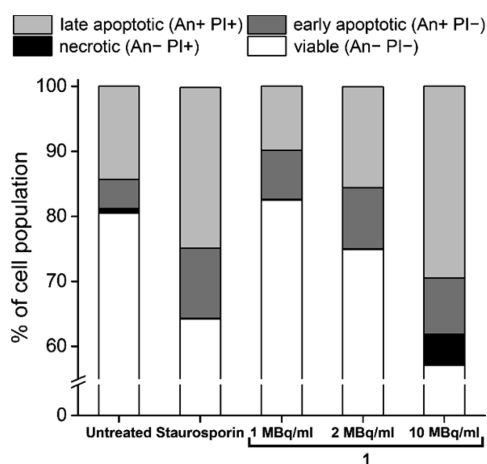


Figure 5. Annexin V (An)/Propidium iodide (PI) assay of **1** in B16F1 cells (72 h incubation time). Staurosporin (5 nM) was used as a positive control.

of early and late apoptotic cells, after treatment with **1** (17.4–38.1%), approached the value of Staurosporin (35.5%) in a dose-dependent fashion, indicating that radiodrug **1** induces apoptosis. It has been shown before that radiation predominantly implicates this programmed cell death pathway.⁸³ Interestingly, raising the concentration of **1** to 10 MBq/mL gave rise to a small percentage of necrotic cells. We assume that at high exposures of radioactivity excessive stress induces to a partial necrotic cell death pathway.

Microdosimetry. To rationalize the observed radiotoxic effect and to illustrate the intracellular dose proportions a microdosimetric evaluation was carried out. The experimental conditions of the radiotoxicity assay were modeled with the

Geant4Monte Carlo toolkit⁸⁴ for the most sensitive B16F1 cell line. Total dose was determined based on the emission spectrum of ^{99m}Tc reported by Howell⁸⁵ and calculation of the energy deposited by disintegrations in the extracellular compartment, cytosol, and nucleus. Calculated dosimetric S -values as well as the time-dependent uptake of **1** are given in Chart S21. Figure 6 depicts the experimentally determined surviving fractions of the radiotoxicity assay vs calculated doses in the nucleus and cytoplasm and the mean cellular dose. At the highest activity concentration of ~ 10 MBq/mL (1 nM in ^{99m}Tc and ^{99}Tc), the nuclear dose is 12.5 Gy. This energy transfer can cause more than 10^6 ionizations per nucleus in 36 h and rationalizes the reduced surviving fraction of 22%. The dose in the cytoplasm is around six times smaller than the dose in the nucleus at equal activity concentrations (see Chart S22), reflecting the cellular distribution of the compound. Nearly identical nuclear doses of a single cell (11.6 Gy) compared to a cell growing in a monolayer (12.5 Gy) demonstrate the preferential accumulation of the radionuclide in the cell nucleus. At ~ 10 MBq/mL, the dose in the extracellular medium is only 0.39 Gy. It is remarkable that more than 99% of the total radioactivity remaining in the medium inflicts a dose which is about 30 times smaller than the nuclear dose. This calculation is further consistent with the survival of 90% for $[^{99m}TcO_4]^-$, which is not taken up by the cells (vide supra). It clearly illustrates that Auger and internal conversion electron emitters like **1**, accumulated in the nucleus, lead to a significant dose and reduced cell survival, whereas the low LET γ -radiation from disintegrations in the medium fails to inflict such damage. The dose–response fit curve in Figure 5 does not depict a shoulder at low doses which is indicative of a high LET-like radiation damage.⁸⁶ These dosimetry considerations thus relate the radiobiology of ultrashort path length radiation to the observed radiotoxicity and connect it to the action of Auger electrons.

In Vivo Evaluation. The in vivo biodistribution and stability of ADR conjugate **1** was evaluated in healthy, nude NMRI mice. Compound **1** was administered intravenously with activity ranging from 8 to 53 MBq per 200 μ L injected volume. A subgroup of mice ($n = 3$) was placed under a microSPECT scanner and imaged in six full body scans, in 10 min frames, from 0 to 60 min post injection (p.i). All mice ($n = 5$) were sacrificed 60 min p.i.

The ex vivo biodistribution analysis (Figure 7) showed a rapid clearance from the blood pool into organs and a remainder of less than 4%ID/g in the blood pool at 60 min p.i. Uptake was most pronounced in the digestive system and excretion organs while other organs of interest exhibited generally low uptake (detailed %ID/g numbers, see Chart S23). The uptake of **1** in the liver suggests a main clearance pathway via the hepatobiliary system, while uptake in the kidneys also evidenced a partial renal clearance. Clearance of the compound into the intestines had already started 1 h p.i., as a large uptake was visible in these organs. RP-HPLC analysis of the blood plasma showed $>80\%$ intact **1** at 1 h p.i., with minor contributions from more hydrophilic metabolites (Chart S24). We tentatively assign the compound at $t_R \approx 4$ min to a low-molecular-weight, hydrophilic metabolite that may be responsible for the uptake in the salivary glands. Blood plasma analysis evidenced a second metabolite in the region of the intact compound. Closer examination (Chart S25) strongly suggested this metabolite to be a reduced species of **1**, containing the Doxorubicinol (Doxol) moiety (Figure 8).

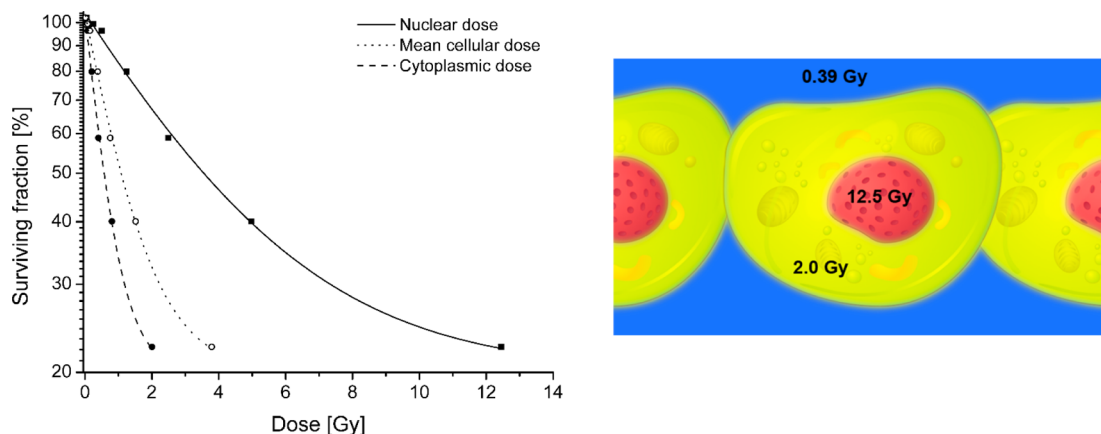


Figure 6. Left: Experimentally evaluated surviving fraction in the B16F1 cell line as a function of dose in the nucleus (■), cytoplasm (●), and averaged whole cell (○). Lines represent monoexponential fits to the calculated values. Right: Illustration of the dose proportions (at 9.25 MBq/mL of **1**) in a cell growing in a monolayer.

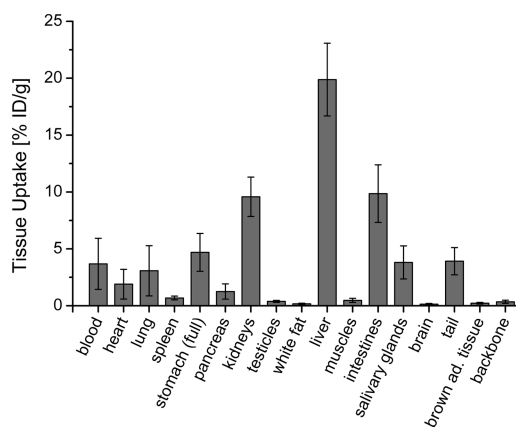


Figure 7. Ex vivo biodistribution of **1** in healthy, nude NMRI mice ($n = 5$, dissection 60 min p.i.). Data is expressed as the mean %-injected dose per gram of tissue (%ID/g) \pm SEM.

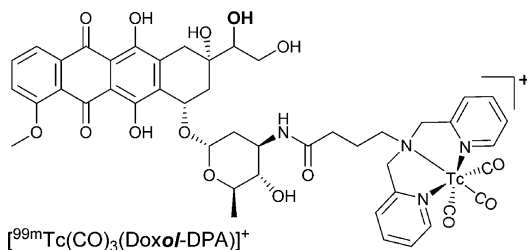


Figure 8. Structure of the proposed Doxorubicin metabolite of **1**.

Doxol is part of the hepatic metabolism of the parent ADR, which arises due to chemoselective reduction by carbonyl reductases in vivo.^{87,88} The metabolite analysis of the urine (total activity recovered 0.26%ID) revealed a multitude of more hydrophilic metabolites with only a small remainder of intact **1** (Chart S22).

Figure 9 shows a representative microSPECT scan of conjugate **1** (frame 6:50–60 min p.i.), which largely reflects the ex vivo biodistribution. The major hepatic assimilation of the compound was already visible 10 min p.i., rationalizing the low blood pool remainder at 60 min p.i. A short blood half-life is known for the parent ADR.⁸⁹ Region of interest (ROI) analysis in the liver throughout the frames indicated a slow clearance of the compound into the intestines. The fast and

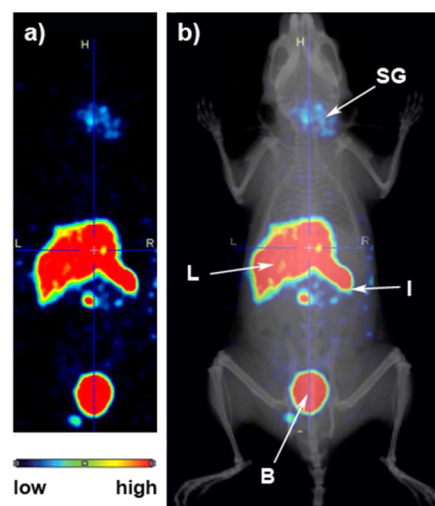


Figure 9. (a) Representative SPECT scan of **1**, frame 6:50–60 min p.i. (b) Overlay of the SPECT scan on a mouse X-ray for better illustration purposes. Visible are liver (L), part of the intestines (I), urinary bladder (B), and salivary glands (SG).

pronounced liver uptake may be attributed to the relative lipophilicity ($\log D_1 = 0.92 \pm 0.03$) and size of conjugate **1**. Moreover, uptake of a radioactive species into the salivary glands was also verified by the SPECT scans. Overall, the collective in vivo data shows close resemblance to the metabolism of free ADR: predominant biotransformation in the liver, biliary excretion through the intestines and, to a minor extent, via the kidneys.⁹⁰ Similarities between free ADR and conjugate **1**, such as hydrophobicity ($\log D_{\text{ADR}} = 0.45 \pm 0.03$)⁹¹ and the “+1” charge at physiological pH, rationalize the comparable in vivo behavior. Of note, the higher lipophilicity of the organometallic ADR derivative compared to ADR could potentially exacerbate the clearance properties of ADR.

CONCLUSION

Doxorubicin (ADR), a routinely applied anticancer pharmaceutical, could serve as a lead structure for targeted molecular imaging or medicinal inorganic drug delivery. We showed that two ADR–metal conjugates ($M = ^{99m}\text{Tc}$, **1** and Re, **2**) mimic the in vitro behavior of ADR. Differences observed in fluorescence microscopy between ADR and **2** enticed a careful

study of the cellular distribution which unambiguously evidenced a major nuclear accumulation. These results advocate caution when assessing the distribution of luminescent compounds in general, as a fluorescence signal by itself may be deceptive and not reflect the true cellular localization.

Furthermore, ^{99m}Tc compound **1** exhibited a dose-dependent reduction of viability of up to 80% in the B16F1 cell line through its Auger electron emission, making this study an important step toward a possible treatment strategy with these low-energy electrons. As demonstrated, Auger emitters may provoke inhibition of cell survival at concentrations which are much lower than the ones of their chemotoxic counterparts. This offers the prospect that conjugates of Auger emitters and chemotherapeutic agents, like **1**, could mitigate dose-dependent adverse effects, as the subnanomolar concentrations likely do not elicit pharmacological responses. For drugs with potent side effects, such as ADR, overcoming these drawbacks could greatly improve therapeutic margins. Multidrug resistance (MDR)^{92–94} and the much-dreaded cardiotoxicity^{95,96} are both concentration-dependent phenomena which can likely be circumvented due to the minute radio-drug concentrations employed in Auger electron therapy. Evidence for this concept has been shown for MDR.⁹⁷

The similarities of conjugate **1** to ADR are an incentive for studies in tumor-bearing mice, allowing for a dosimetric evaluation in vivo and an assessment of the validity of the proposed system in the treatment regime. Furthermore, clonogenic assays will provide insights into long-term viability of the cells. Such studies, in addition to alternative constructs with different chelating units, are currently ongoing.

■ ASSOCIATED CONTENT

📄 Supporting Information

The Supporting Information is available free of charge on the ACS Publications website at DOI: 10.1021/acs.bioconjchem.5b00466.

Materials and methods (PDF)

■ AUTHOR INFORMATION

Corresponding Author

*E-mail: ariel@chem.uzh.ch. Tel.: +41-52-635 46 31.

Notes

The authors declare no competing financial interest.

■ ACKNOWLEDGMENTS

We gratefully acknowledge M. De Saint-Hubert, I. Pooters, S. Voo, and R. Wierth from the MUMC+ for their care during the in vivo evaluation, F. Wild for ICP-MS measurements, and the Graduate School of Chemical and Molecular Sciences Zurich (CMSZH) for a travel grant. M. Bauwens is supported by the Weijerhorst Foundation. This work was financially supported by the Swiss National Science Foundation (Professorships No PP00P2_133568 and PP00P2_157545 to G.G.), the University of Zurich (G.G. and R.A.), the Stiftung für Wissenschaftliche Forschung of the University of Zurich (G.G.), and an SBF1 grant C13.0080 (COST Action CM1105).

■ REFERENCES

(1) Pouget, J.-P.; Navarro-Teulon, I.; Bardies, M.; Chouin, N.; Cartron, G.; Pelegrin, A.; and Azria, D. (2011) Clinical radioimmunotherapy—the role of radiobiology. *Nat. Rev. Clin. Oncol.* 8, 720–734.

(2) Howell, R. W., Rao, D. V., Hou, D. Y., Narra, V. R., and Sastry, K. S. R. (1991) The question of relative biological effectiveness and quality factor for Auger emitters incorporated into proliferating mammalian cells. *Radiat. Res.* 128, 282–292.

(3) Bloomer, W. D., and Adelstein, S. J. (1977) 5-I-125-Iododeoxyuridine as prototype for radionuclide therapy with Auger emitters. *Nature* 265, 620–621.

(4) Painter, R. B., Young, B. R., and Burki, H. J. (1974) Non-Repairable Strand Breaks Induced by I-125 Incorporated into Mammalian DNA. *Proc. Natl. Acad. Sci. U. S. A.* 71, 4836–4838.

(5) Panyutin, I. G., and Neumann, R. D. (1994) Sequence-Specific DNA Double-Strand Breaks Induced by Triplex Forming I-125 Labeled Oligonucleotides. *Nucleic Acids Res.* 22, 4979–4982.

(6) Schneiderman, M. H., and Schneiderman, G. S. (1996) Radioiododeoxyuridine in cancer therapy: An in vitro approach to developing in vivo strategies. *J. Nucl. Med.* 37, S6–S9.

(7) McLaughlin, W. H., Milius, R. A., Pillai, K. M. R., Edasery, J. P., Blumenthal, R. D., and Bloomer, W. D. (1989) Cyto-Toxicity of Receptor-Mediated 16-Alpha-[I-125]Iodo-Estradiol in Cultured MCF-7 Human-Breast Cancer-Cells. *J. Natl. Cancer I* 81, 437–440.

(8) Desombre, E. R., Shafii, B., Hanson, R. N., Kuivanen, P. C., and Hughes, A. (1992) Estrogen receptor directed radiotoxicity with Auger electrons - specificity and mean lethal dose. *Cancer Res.* 52, 5752–5758.

(9) Kassis, A. I., Fayad, F., Kinsey, B. M., Sastry, K. S. R., and Adelstein, S. J. (1989) Radiotoxicity of an I-125-Labeled DNA Intercalator in Mammalian-Cells. *Radiat. Res.* 118, 283–294.

(10) Hofer, K. G. (2000) Biophysical aspects of Auger processes. *Acta Oncol.* 39, 651–657.

(11) Kassis, A. I. (2003) Cancer therapy with auger electrons: are we almost there? *J. Nucl. Med.* 44, 1479–1481.

(12) Pillai, M. R. A., Dash, A., and Knapp, F. F., Jr. (2013) Sustained Availability of Tc-99m: Possible Paths Forward. *J. Nucl. Med.* 54, 313–323.

(13) Tavares, A. A. S., and Tavares, J. M. R. S. (2010) Tc-99m Auger electrons for targeted tumour therapy: A review. *Int. J. Radiat. Biol.* 86, 261–270.

(14) Ftacnikova, S., and Bohm, R. (2000) Monte Carlo calculations of energy deposition in DNA for Auger emitters. *Radiat. Prot. Dosim.* 92, 269–278.

(15) Haefliger, P., Agorastos, N., Spingler, B., Georgiev, O., Viola, G., and Alberto, R. (2005) Induction of DNA-double-strand breaks by Auger electrons from Tc-99m complexes with DNA-binding ligands. *ChemBioChem* 6, 414–421.

(16) Kotzerke, J., Punzet, R., Runge, R., Ferl, S., Oehme, L., Wunderlich, G., and Freudenberg, R. (2014) ^{99m}Tc -Labeled HYNIC-DAPI Causes Plasmid DNA Damage with High Efficiency. *PLoS One* 9, e104653.

(17) Haefliger, P., Agorastos, N., Renard, A., Giambonini-Brugnoli, G., Marty, C., and Alberto, R. (2005) Cell uptake and radiotoxicity studies of an nuclear localization signal peptide-intercalator conjugate labeled with $[\text{Tc-}^{99m}(\text{CO})(3)](+)$. *Bioconjugate Chem.* 16, 582–587.

(18) Vitor, R. F., Esteves, T., Marques, F., Raposo, P., Paulo, A., Rodrigues, S., Rueff, J., Casimiro, S., Costa, L., and Santos, I. (2009) Tc-99m-Tricarbonyl Complexes Functionalized with Anthracenyl Fragments: Synthesis, Characterization, and Evaluation of Their Radiotoxic Effects in Murine Melanoma Cells. *Cancer Biother.Radiopharm.* 24, 551–563.

(19) Arcamone, F., Franceschi, G., Penco, S., and Selva, A. (1969) Adriamycin (14-Hydroxydaunomycin) a Novel Antitumor Antibiotic. *Tetrahedron Lett.* 10, 1007–1010.

(20) Arcamone, F., Cassinelli, G., Fantini, G., Grein, A., Orezzi, P., Pol, C., and Spalla, C. (2000) Adriamycin, 14-hydroxydaunomycin, a new antitumor antibiotic from *S. peucetius* var. *caesius* (Reprinted from Biotechnology and Bioengineering. *Biotechnol. Bioeng.* 67, 704–713.

(21) Waring, M. J. (1981) DNA modification and cancer. *Annu. Rev. Biochem.* 50, 159–192.

- (22) Lown, J. W. (1993) Discovery and development of anthracycline antitumor antibiotics. *Chem. Soc. Rev.* 22, 165–176.
- (23) Carvalho, C., Santos, R. X., Cardoso, S., Correia, S., Oliveira, P. J., Santos, M. S., and Moreira, P. I. (2009) Doxorubicin: The Good, the Bad and the Ugly Effect. *Curr. Med. Chem.* 16, 3267–3285.
- (24) Minotti, G., Menna, P., Salvatorelli, E., Cairo, G., and Gianni, L. (2004) Anthracyclines: Molecular advances and pharmacologic developments in antitumor activity and cardiotoxicity. *Pharmacol. Rev.* 56, 185–229.
- (25) Gewirtz, D. A. (1999) A critical evaluation of the mechanisms of action proposed for the antitumor effects of the anthracycline antibiotics Adriamycin and daunorubicin. *Biochem. Pharmacol.* 57, 727–741.
- (26) Shepherd, G. M. (2003) Hypersensitivity reactions to chemotherapeutic drugs. *Clin. Rev. Allergy Immunol.* 24, 253–262.
- (27) Sonis, S. T., Elting, L. S., Keefe, D., Peterson, D. E., Schubert, M., Hauer-Jensen, M., Bekele, B. N., Raber-Durlacher, J., Donnelly, J. P., and Rubenstein, E. B. (2004) Perspectives on cancer therapy-induced mucosal injury - Pathogenesis, measurement, epidemiology, and consequences for patients. *Cancer* 100, 1995–2025.
- (28) Juliano, R. L., and Stamp, D. (1975) Effect of particle size and charge on clearance rates of liposomes encapsulated drugs. *Biochem. Biophys. Res. Commun.* 63, 651–658.
- (29) Poste, G., Bucana, C., Raz, A., Bugelski, P., Kirsh, R., and Fidler, I. J. (1982) Analysis of the fate of systematically administered liposomes and implications for their use in drug delivery. *Cancer Res.* 42, 1412–1422.
- (30) Gabizon, A., Shmeeda, H., and Barenholz, Y. (2003) Pharmacokinetics of pegylated liposomal doxorubicin - Review of animal and human studies. *Clin. Pharmacokinet.* 42, 419–436.
- (31) Ta, H. T., Dass, C. R., Larson, I., Choong, P. F. M., and Dunstan, D. E. (2009) A chitosan-dipotassium orthophosphate hydrogel for the delivery of Doxorubicin in the treatment of osteosarcoma. *Biomaterials* 30, 3605–3613.
- (32) Ta, H. T., Han, H., Larson, I., Dass, C. R., and Dunstan, D. E. (2009) Chitosan-dibasic orthophosphate hydrogel: A potential drug delivery system. *Int. J. Pharm.* 371, 134–141.
- (33) Tan, M. L., Friedhuber, A. M., Dunstan, D. E., Choong, P. F. M., and Dass, C. R. (2010) The performance of doxorubicin encapsulated in chitosan-dextran sulphate microparticles in an osteosarcoma model. *Biomaterials* 31, 541–551.
- (34) Mitra, S., Gaur, U., Ghosh, P. C., and Maitra, A. N. (2001) Tumor targeted delivery of encapsulated dextran-doxorubicin conjugate using chitosan nanoparticles as carrier. *J. Controlled Release* 74, 317–323.
- (35) Sun, K., Wang, J., Zhang, J., Hua, M., Liu, C., and Chen, T. (2011) Dextran-g-PEI nanoparticles as a carrier for co-delivery of adriamycin and plasmid into osteosarcoma cells. *Int. J. Biol. Macromol.* 49, 173–180.
- (36) Monem, A. S., Elbially, N., and Mohamed, N. (2014) Mesoporous silica coated gold nanorods loaded doxorubicin for combined chemo-photothermal therapy. *Int. J. Pharm.* 470, 1–7.
- (37) Joseph, M. M., Aravind, S. R., George, S. K., Pillai, K. R., Mini, S., and Sreelekha, T. T. (2014) Galactoxylglucan-Modified Nano-carriers of Doxorubicin for Improved Tumor-Targeted Drug Delivery with Minimal Toxicity. *J. Biomed. Nanotechnol.* 10, 3253–3268.
- (38) Farquhar, D., Cherif, A., Bakina, E., and Nelson, J. A. (1998) Intensely potent doxorubicin analogues: Structure-activity relationship. *J. Med. Chem.* 41, 965–972.
- (39) DeFeo-Jones, D., Garsky, V. M., Wong, B. K., Feng, D. M., Bolyar, T., Haskell, K., Kiefer, D. M., Leander, K., McAvoy, E., Lumma, P., et al. (2000) A peptide-doxorubicin 'prodrug' activated by prostate-specific antigen selectively kills prostate tumor cells positive for prostate-specific antigen in vivo. *Nat. Med.* 6, 1248–1252.
- (40) Ibsen, S., Zahavy, E., Wrasidlo, W., Hayashi, T., Norton, J., Su, Y., Adams, S., and Esener, S. (2013) Localized In Vivo Activation of a Photoactivatable Doxorubicin Prodrug in Deep Tumor Tissue. *Photochem. Photobiol.* 89, 698–708.
- (41) Volker, T., Dempwolff, F., Graumann, P. L., and Meggers, E. (2014) Progress towards bioorthogonal catalysis with organometallic compounds. *Angew. Chem., Int. Ed.* 53, 10536–40.
- (42) Damen, E. W. P., de Groot, F. M. H., and Scheeren, H. W. (2001) Novel anthracycline prodrugs. *Expert Opin. Ther. Pat.* 11, 651–666.
- (43) Ramogida, C. F., and Orvig, C. (2013) Tumor targeting with radiometals for diagnosis and therapy. *Chem. Commun.* 49, 4720–4739.
- (44) Levadala, M. K., Banerjee, S. R., Maresca, K. P., Babich, J. W., and Zubieta, J. (2004) Direct reductive alkylation of amino acids: Synthesis of bifunctional chelates for nuclear imaging. *Synthesis* 2004, 1759–1766.
- (45) Robert, J., and Gianni, L. (1993) Pharmacokinetics and metabolism of anthracyclines. *Cancer Surv.* 17, 219–252.
- (46) Licata, S., Saponiero, A., Mordente, A., and Minotti, G. (2000) Doxorubicin metabolism and toxicity in human myocardium: Role of cytoplasmic deglycosidation and carbonyl reduction. *Chem. Res. Toxicol.* 13, 414–420.
- (47) Cortesfunes, H., Gosalvez, M., Moyano, A., Manas, A., and Mendiola, C. (1979) Early clinical trial with quelamycin. *Cancer Treat. Rep.* 63, 903–907.
- (48) Cortes, H., Vicente, J., Baena, L., Otero, J., and Gosalvez, M. (1978) Preliminary evaluation of a phase-I clinical study of quelamycin. *Eur. J. Cancer* 14, 1359–1361.
- (49) Cortesfunes, H., Brugarolas, A., and Gosalvez, M. (1980) Quelamycin - a summary of phase-I clinical trials. *Recent Results Cancer Res.* 74, 200–206.
- (50) Gosalvez, M., Blanco, M. F., Vivero, C., and Valles, F. (1978) Quelamycin, a new derivative of adriamycin with several possible therapeutic advantages. *Eur. J. Cancer* 14, 1185–1190.
- (51) Abraham, S. A., Edwards, K., Karlsson, G., MacIntosh, S., Mayer, L. D., McKenzie, C., and Bally, M. B. (2002) Formation of transition metal-doxorubicin complexes inside liposomes. *Biochim. Biophys. Acta, Biomembr.* 1565, 41–54.
- (52) Monti, E., Paracchini, L., Piccinini, F., Malatesta, V., Morazzoni, F., and Supino, R. (1990) Cardiotoxicity and antitumor activity of a copper(II) doxorubicin chelate. *Cancer Chemother. Pharmacol.* 25, 333–336.
- (53) Zunino, F., Pratesi, G., Formelli, F., and Pasini, A. (1990) Evaluation of platinum-doxorubicin complex in experimental tumor systems. *Invest. New Drugs* 8, 341–345.
- (54) Tachibana, M., Iwaizumi, M., and Terokubota, S. (1987) Electron paramagnetic resonance studies of copper(II) and cobalt(II) complexes of adriamycin. *J. Inorg. Biochem.* 30, 133–140.
- (55) Fiallo, M. M. L., and Garniersuillerot, A. (1986) Metal anthracycline complexes as a new class of anthracycline derivatives, Pd(II)-adriamycin and Pd(II) daunorubicin complexes- physicochemical characteristics and antitumor activity. *Biochemistry* 25, 924–930.
- (56) Rizvi, F. A., Bokhari, T. H., Roohi, S., and Mushtaq, A. (2012) Direct labeling of doxorubicin with technetium-99m: its optimization, characterization and quality control. *J. Radioanal. Nucl. Chem.* 293, 303–307.
- (57) Kassis, A. I., Sastry, K. S. R., and Adelstein, S. J. (1987) Kinetics of Uptake, Retention, and Radiotoxicity of I-125 Udr in Mammalian-Cells - Implications of Localized Energy Deposition by Auger Processes. *Radiat. Res.* 109, 78–89.
- (58) Balagurumoorthy, P., Xu, X., Wang, K., Adelstein, S. J., and Kassis, A. I. (2012) Effect of distance between decaying I-125 and DNA on Auger-electron induced double-strand break yield. *Int. J. Radiat. Biol.* 88, 998–1008.
- (59) Barcelo, F., Martorell, J., Gavilanes, F., and Gonzalezros, J. M. (1988) Equilibrium binding of daunomycin and adriamycin to calf thymus DNA - temperature and ionic-strength dependence of thermodynamic parameters. *Biochem. Pharmacol.* 37, 2133–2138.
- (60) Carter, M. T., Rodriguez, M., and Bard, A. J. (1989) Voltametric studies of the interaction of metal-chelates with DNA. 2. Tris-chelated complexes of cobalt(III) and iron(II) with 1,10-phenantroline and 2,2'-bipyridine. *J. Am. Chem. Soc.* 111, 8901–8911.

- (61) Kalsbeck, W. A., and Thorp, H. H. (1993) Determining Binding Constants of Metal-Complexes to DNA by Quenching of the Emission of Pt₂(Pop)₄(4-) (Pop = P₂O₅H₂₂-). *J. Am. Chem. Soc.* *115*, 7146–7151.
- (62) Dimarco, A., and Arcamone, F. (1975) DNA complexing daunomycin, adriamycin and their derivatives. *Arzneim.-Forsch.* *25*, 368–375.
- (63) Matikonda, S. S., Orsi, D. L., Staudacher, V., Jenkins, I. A., Fiedler, F., Chen, J., and Gamble, A. B. (2015) Bioorthogonal prodrug activation driven by a strain-promoted 1,3-dipolar cycloaddition. *Chem. Sci.* *6*, 1212–1218.
- (64) Top, S., Vessieres, A., Pigeon, P., Rager, M. N., Huche, M., Salomon, E., Cabestaing, C., Vaissermann, J., and Jaouen, G. (2004) Selective estrogen-receptor modulators (SERMs) in the cyclopentadienylrhenium tricarbonyl series: Synthesis and biological behaviour. *ChemBioChem* *5*, 1104–1113.
- (65) Bartholomae, M. D., Vortherms, A. R., Hillier, S., Joyal, J., Babich, J., Doyle, R. P., and Zubieta, J. (2011) Synthesis, cytotoxicity and cellular uptake studies of N3 functionalized Re(CO)₃ thymidine complexes. *Dalton Trans.* *40*, 6216–6225.
- (66) Parson, C., Smith, V., Krauss, C., Banerjee, H. N., Reilly, C., Krause, J. A., Wachira, J. M., Giri, D., Winstead, A., and Mandal, S. K. (2015) Anticancer Properties of Novel Rhenium Pentylcarbanato Compounds against MDA-MB-468(HTB-132) Triple Node Negative Human Breast Cancer Cell Lines. *Br. J. Pharm. Res.* *4*, 362–7.
- (67) Leonidova, A., and Gasser, G. (2014) Underestimated Potential of Organometallic Rhenium Complexes as Anticancer Agents. *ACS Chem. Biol.* *9*, 2180–2193.
- (68) Pommier, Y., Leo, E., Zhang, H., and Marchand, C. (2010) DNA Topoisomerases and Their Poisoning by Anticancer and Antibacterial Drugs. *Chem. Biol.* *17*, 421–433.
- (69) Shapiro, A. B., and Austin, C. A. (2014) A high-throughput fluorescence anisotropy-based assay for human topoisomerase II beta-catalyzed ATP-dependent supercoiled DNA relaxation. *Anal. Biochem.* *448*, 23–29.
- (70) Shapiro, A. B. (2013) A high-throughput-compatible, fluorescence anisotropy-based assay for ATP-dependent supercoiled DNA relaxation by human topoisomerase II alpha. *Biochem. Pharmacol.* *85*, 1269–1277.
- (71) Hofer, K. G., Harris, C. R., and Smith, J. M. (1975) Radiotoxicity of intracellular Ga-67, I-125 and H-3, nuclear versus cytoplasmic radiation effects in murine L1210 leukemia. *Int. J. Radiat. Biol.* *28*, 225–241.
- (72) Warters, R. L., and Hofer, K. G. (1977) Radionuclide toxicity in cultured mammalian cells. elucidation of primary site for radiation induced division delay. *Radiat. Res.* *69*, 348–358.
- (73) Jonkhoff, A. R., Vondieren, E. B., Huijgens, P. C., Versteegh, R. T., Drager, A., Vanderloosdrecht, A. A., and Teule, G. J. J. (1994) Biological effectiveness of Ga-67 decay in HL-60 cells compared with external low-dose rate gamma radiation - effects on proliferation, G2 arrest and clonogenic capacity. *Int. J. Radiat. Oncol., Biol., Phys.* *30*, 117–124.
- (74) Narra, V. R., Howell, R. W., Harapanhalli, R. S., Sastry, K. S. R., and Rao, D. V. (1992) Radiotoxicity of some I-123, I-125 and Iodine-131-labeled compounds in mouse testes - implications for radiopharmaceutical design. *J. Nucl. Med.* *33*, 2196–2201.
- (75) Mohan, P., and Rapoport, N. (2010) Doxorubicin as a Molecular Nanotheranostic Agent: Effect of Doxorubicin Encapsulation in Micelles or Nanoemulsions on the Ultrasound-Mediated Intracellular Delivery and Nuclear Trafficking. *Mol. Pharmaceutics* *7*, 1959–1973.
- (76) Gigli, M., Rasoanaivo, T. W. D., Millot, J. M., Jeannesson, P., Rizzo, V., Jardillier, J. C., Arcamone, F., and Manfait, M. (1989) Correlation between growth inhibition and intranuclear doxorubicin and 4'-deoxy-4'-iododoxorubicin quantitated in living K562 cells by microspectrofluorometry. *Cancer Res.* *49*, S60–S64.
- (77) Juergens, S., Herrmann, W. A., and Kuehn, F. E. (2014) Rhenium and technetium based radiopharmaceuticals: Development and recent advances. *J. Organomet. Chem.* *751*, 83–89.
- (78) Gianferrara, T., Spagnul, C., Alberto, R., Gasser, G., Ferrari, S., Pierroz, V., Bergamo, A., and Alessio, E. (2014) Towards matched pairs of porphyrin-Re(I) / (99m) Tc(I) conjugates that combine photodynamic activity with fluorescence and radio imaging. *Chem-MedChem* *9*, 1231–7.
- (79) Agorastos, N., Borsig, L., Renard, A., Antoni, P., Viola, G., Spingler, B., Kurz, P., and Alberto, R. (2007) Cell-specific and nuclear targeting with [M(CO)₃](+) (M = Tc-99m, Re)-based complexes conjugated to acridine orange and bombesin. *Chem. - Eur. J.* *13*, 3842–3852.
- (80) Fertil, B., and Malaise, E.-P. (1981) Inherent cellular radiosensitivity as a basic concept for human tumor radiotherapy. *Int. J. Radiat. Oncol., Biol., Phys.* *7*, 621–629.
- (81) Rosen, E. M., Fan, S., Rockwell, S., and Goldberg, I. D. (1999) The molecular and cellular basis of radiosensitivity: implications for understanding how normal tissues and tumors respond to therapeutic radiation. *Cancer Invest.* *17*, 56–72.
- (82) Belmokhtar, C. A., Hillion, J., and Segal-Bendirdjian, E. (2001) Staurosporine induces apoptosis through both caspase-dependent and caspase-independent mechanisms. *Oncogene* *20*, 3354–3362.
- (83) Verheij, M., and Bartelink, H. (2000) Radiation-induced apoptosis. *Cell Tissue Res.* *301*, 133–142.
- (84) Freudenberger, R., Wendisch, M., and Kotzerke, J. (2011) Geant4-Simulations for cellular dosimetry in nuclear medicine. *Z. Med. Phys.* *21*, 281–289.
- (85) Howell, R. W. (1992) Radiation spectra of Auger-electron emitting radionuclides - report No 2 of AAPM nuclear medicine task group No6. *Med. Phys.* *19*, 1371–1383.
- (86) Hofer, K. G. (1998) Dosimetry and biological effects of incorporated auger emitters. *Radiat. Prot. Dosim.* *79*, 405–410.
- (87) Schaupp, C. M., White, C. C., Merrill, G. F., and Kavanagh, T. J. (2015) Metabolism of doxorubicin to the cardiotoxic metabolite doxorubicinol is increased in a mouse model of chronic glutathione deficiency: A potential role for carbonyl reductase 3. *Chem.-Biol. Interact.* *234*, 154.
- (88) Kassner, N., Huse, K., Martin, H.-J., Gödtel-Armbrust, U., Metzger, A., Meineke, I., Brockmüller, J., Klein, K., Zanger, U. M., Maser, E., et al. (2008) Carbonyl Reductase 1 Is a Predominant Doxorubicin Reductase in the Human Liver. *Drug Metab. Dispos.* *36*, 2113–2120.
- (89) Rahman, A., Carmichael, D., Harris, M., and Roh, J. K. (1986) Comparative pharmacokinetics of free doxorubicin and doxorubicin entrapped in cardiopilin liposomes. *Cancer Res.* *46*, 2295–2299.
- (90) Lal, S., Mahajan, A., Chen, W. N., and Chowbay, B. (2010) Pharmacogenetics of Target Genes Across Doxorubicin Disposition Pathway: A Review. *Curr. Drug Metab.* *11*, 115–128.
- (91) Rousselle, C., Clair, P., Lefauconnier, J.-M., Kaczorek, M., Scherrmann, J.-M., and Tamsamani, J. (2000) New advances in the transport of doxorubicin through the blood-brain barrier by a peptide vector-mediated strategy. *Mol. Pharmacol.* *57*, 679–686.
- (92) Mankhetkorn, S., Dubru, F., Hesschenbrouck, J., Fiallo, M., and Garnier-Suillerot, A. (1996) Relation among the resistance factor, kinetics of uptake, and kinetics of the P-glycoprotein-mediated efflux of doxorubicin, daunorubicin, 8-(S)-fluoroidarubicin, and idarubicin in multidrug-resistant K562 cells. *Mol. Pharmacol.* *49*, 532–9.
- (93) Gottesman, M. M., and Pastan, I. (1993) Biochemistry of Multidrug Resistance Mediated by the Multidrug Transporter. *Annu. Rev. Biochem.* *62*, 385–427.
- (94) Riordan, J. R., and Ling, V. (1985) Genetic and biochemical characterization of multidrug resistance. *Pharmacol. Ther.* *28*, 51–75.
- (95) Lefrak, E. A., Pitha, J., Rosenheim, S., and Gottlieb, J. A. (1973) A clinicopathologic analysis of adriamycin cardiotoxicity. *Cancer* *32*, 302–14.
- (96) Chatterjee, K., Zhang, J., Honbo, N., and Karliner, J. S. (2010) Doxorubicin Cardiomyopathy. *Cardiology* *115*, 155–162.
- (97) Morgenroth, A., Dinger, C., Zlatopolskiy, B. D., Al-Momani, E., Glatting, G., Mottaghy, F. M., and Reske, S. N. (2011) Auger electron emitter against multiple myeloma-targeted endo-radio-therapy with

¹²⁵I-labeled thymidine analogue 5-iodo-4'-thio-2'-deoxyuridine. *Nucl. Med. Biol.* 38, 1067–77.